Globally observed trends in mean and extreme river flow attributed to climate change

Article *in* Science · March 2021

DOI: 10.1126/science.aba3996

17 authors, including:

Lukas Gudmundsson
ETH Zurich
116 PUBLICATIONS **4,064** CITATIONS
SEE PROFILE

Hong Xuan Do
Nong Lam University
33 PUBLICATIONS **576** CITATIONS
SEE PROFILE

Simon Gosling
University of Nottingham
131 PUBLICATIONS **9,369** CITATIONS
SEE PROFILE

Manolis Grillakis
Foundation for Research and Technology - Hellas
98 PUBLICATIONS **1,484** CITATIONS
SEE PROFILE

HYDROLOGY

Globally observed trends in mean and extreme river flow attributed to climate change

Lukas Gudmundsson[1]*, Julien Boulange[2], Hong X. Do[3,4,5], Simon N. Gosling[6], Manolis G. Grillakis[7], Aristeidis G. Koutroulis[8], Michael Leonard[3], Junguo Liu[9], Hannes Müller Schmied[10,11], Lamprini Papadimitriou[12,13], Yadu Pokhrel[14], Sonia I. Seneviratne[1], Yusuke Satoh[2,15], Wim Thiery[1,16], Seth Westra[3], Xuebin Zhang[17], Fang Zhao[18,19]

Anthropogenic climate change is expected to affect global river flow. Here, we analyze time series of low, mean, and high river flows from 7250 observatories around the world covering the years 1971 to 2010. We identify spatially complex trend patterns, where some regions are drying and others are wetting consistently across low, mean, and high flows. Trends computed from state-of-the-art model simulations are consistent with the observations only if radiative forcing that accounts for anthropogenic climate change is considered. Simulated effects of water and land management do not suffice to reproduce the observed trend pattern. Thus, the analysis provides clear evidence for the role of externally forced climate change as a causal driver of recent trends in mean and extreme river flow at the global scale.

Among key concerns with respect to anthropogenic climate change (ACC) are impacts on the terrestrial water cycle. Earth system models (ESMs) indicate that projected ACC can influence water availability on land (*1*) and may trigger more floods (*2*) and droughts (*3*). Although detection and attribution studies have shown that observed changes in atmospheric variables such as precipitation (*4*, *5*) and water vapor (*6*) are consistent with model simulations that account for historical ACC, evidence for a human fingerprint on past changes in river flow and hydrological extremes is still lacking at the global scale.

Two factors have complicated the detection and attribution of changes in terrestrial water systems at the global scale. First, although river flow time series are the most abundant observations of water resources and hydrological extremes, the slow mobilization of in situ observations has confined past assessments to regional and continental case studies (*7*–*12*) or to small collections of large river basins, with most of the records ending in the 20th century (*13*–*15*). To circumvent this lack of global in situ observations, researchers have used reconstructions of essential hydrological variables such as soil moisture (*16*–*18*) or evapotranspiration (*19*) and indicators of water availability (*20*) as the basis for climate change detection and attribution studies. Although these efforts have revealed that ACC is detectable in terrestrial water systems, they lack a direct connection to in situ observations of quantities relevant for water management.

Second, besides ACC, on-ground human activities such as historical water and land management (HWLM) are also altering water resources and hydrological extremes, e.g., directly through flow regulation and water abstractions or indirectly through effects of land-cover change (*13*). For example, large-scale water withdrawal for irrigation might induce declining trends in river flow. Likewise, reservoir expansion may lead to changes in stream flow. Several studies have shown that effects of HWLM on water resources could be equally large or might even exceed climate change impacts in some regions (*13*, *21*, *22*). However, ESMs, which are an important tool for attributing observed changes to human influences on the climate system, typically do not account for HWLM as a possible confounding factor (*7*).

Recent advances in mobilizing in situ river flow observations (*23*, *24*) and an unprecedented multimodel ensemble that combines the ESMs' ability to account for ACC with the capacity of high-resolution global hydrology models (GHMs) to incorporate HWLM (*25*) allow us to tackle the challenge of attributing observed changes in river flow at the global scale. Here, we consider in situ observations of daily average river flow from 7250 gauging stations (fig. S1) that have at least 28 years with almost complete daily data from 1971 to 2010 (*26*). To balance the uneven spatial distribution of in situ observations, the analysis is constrained to predefined subcontinental regions (*27*) with at least 80 stations. Yearly time series of low (annual 10th percentile), mean (annual mean), and high (annual 90th percentile) river flows are considered, respectively representing very dry, average, and very wet conditions. For each time series, trends are estimated and expressed in terms of percentage change per decade. Subsequently, the median trend is computed for each region to reduce the effects of local-scale natural variability, observational errors, and spatial autocorrelation for further statistical analyses (*28*).

Figure 1 reveals spatially complex trend patterns in observed low, mean, and high river flow. Some regions such as northeast Brazil, southern Australia, and the Mediterranean show a drying tendency. Other regions such as northern Europe tend toward wetter conditions. We also note that the level of spatial aggregation may mask subregional differences. The analysis also confirms previous results (*29*) indicating that the direction of change is often consistent throughout the entire flow distribution, i.e., trends in low, mean, and high flows share the same sign. Reconstructions of global river flow from the Inter-Sectoral Impact Model Intercomparison Project phase 2a (ISIMIP2a) that are based on GHMs driven with observational atmospheric data (*30*) are highly correlated with the observed trend pattern (Fig. 1), although the reconstructions have a tendency to underestimate the magnitude of the observed trends. Accounting for HWLM does not improve the skill of the reconstruction in reproducing the spatial patterns of observed regional median trends, even though it can improve overall model performance (*31*).

Although the above assessment shows that changes in the atmospheric conditions are driving observed trends in low, mean, and high river flow, it remains unclear if these changes can be attributed to ACC. To tackle this question, we used the climate change detection and attribution approach (*32*), which ingests both observations and simulation experiments that include or exclude the drivers of ACC. If (i) simulations that include the drivers of ACC are consistent with the observations and (ii) simulations that do not include them fail to be consistent with the observations, then it is possible to claim attribution. Here, we consider two simulation experiments from the Inter-Sectoral Impact Model Intercomparison Project phase 2b (ISIMIP2b) (*25*),

[1]Institute for Atmospheric and Climate Science, Department of Environmental Systems Science, ETH Zurich, Zürich, Switzerland. [2]National Institute for Environmental Studies (NIES), Tsukuba, Japan. [3]School of Civil, Environmental and Mining Engineering, University of Adelaide, Adelaide, SA, Australia. [4]Faculty of Environment and Natural Resources, Nong Lam University, Ho Chi Minh City, Vietnam. [5]School for Environment and Sustainability, University of Michigan, Ann Arbor, MI, USA. [6]School of Geography, University of Nottingham, Nottingham NG7 2RD, UK. [7]Institute for Mediterranean Studies, Foundation for Research and Technology Hellas, Rethymno 74100, Greece. [8]School of Environmental Engineering, Technical University of Crete, Chania, Greece. [9]School of Environmental Science and Engineering, Southern University of Science and Technology (SUSTech), Shenzhen 518055, China. [10]Institute of Physical Geography, Goethe University Frankfurt, Frankfurt am Main, Germany. [11]Senckenberg Leibniz Biodiversity and Climate Research Centre (SBiK-F), Frankfurt am Main, Germany. [12]Cranfield Water Science Institute, Cranfield University, Cranfield, UK. [13]Mott MacDonald Ltd, Cambridge, UK. [14]Department of Civil and Environmental Engineering, Michigan State University, East Lansing, MI, USA. [15]International Institute for Applied Systems Analysis, Laxenburg, Austria. [16]Department of Hydrology and Hydraulic Engineering, Vrije Universiteit Brussel, Brussels, Belgium. [17]Environment Canada, Toronto, ON, Canada. [18]Key Laboratory of Geographic Information Science (Ministry of Education), School of Geographic Sciences, East China Normal University, Shanghai, China. [19]Potsdam Institute for Climate Impact Research (PIK), Potsdam, Germany.
*Corresponding author. Email: lukas.gudmundsson@env.ethz.ch

where GHMs that account for HWLM are driven with output from ESMs that ingest different radiative forcing. The first experiment considers preindustrial radiative forcing and is referred to as PIC&HWLM from here onward. Because preindustrial radiative forcing does not impose systematic trends in the simulations, the PIC&HWLM experiment allows us to test the hypothesis of whether the observed trend patterns can be explained by the simulated effects of HWLM alone. The second experiment considers historical radiative forcing, which includes both anthropogenic (e.g., human greenhouse gas or aerosol emissions) as well as natural (e.g., influence of large volcanic eruptions) factors throughout the past century. This experiment is referred to as HIST&HWLM and allows us to test the hypothesis of whether the addition of historical radiative forcing contributes to explaining the observed trend pattern.

Figure 2 compares observed river flow trends to trends from both the PIC&HWLM and the HIST&HWLM simulations. The consistency of the observed trend pattern with either of the simulation results is tested using optimal fingerprinting (*28*, *33*). To this end, the multimodel mean of the simulations (x) is regressed on the observations (y) while accounting for natural variability (ϵ) as well as model and sampling errors (ν), such that $y = \beta \times (x - \nu) + \epsilon$ (*33*). Testing the significance of the association between the observed and simulated patterns is based on the magnitude of the scaling factor β. The simulated pattern is said to be detected in the observations if β is significantly larger than zero, i.e., if the lower ends of the associated confidence intervals are above zero. Scaling factors derived from simulations with PIC&HWLM are never significantly larger than zero (Fig. 2). This shows that simulated effects of HWLM without accounting for historical radiative forcing cannot explain the observed trend pattern. This is in agreement with the above assessment, where accounting for HWLM did not improve the consistency of observed and reconstructed trends (Fig. 1). The situation differs for the analysis of HIST&HWLM, i.e., the simulations that account for historical radiative forcing. Here, the scaling factors of all indices are significantly larger than zero ($p < 0.1$).

The results show that the combined effect of historical radiative forcing and HWLM is detected in observed trend patterns of low, mean, and high river flow. The analysis also suggests that the magnitude of the simulated trend patterns under historical radiative forcing is consistent with the observations ($\beta \approx 1$). This, in combination with the finding that accounting for HWLM does not improve reconstructions (Fig. 1), implies that simulated impacts of HWLM only have a minor effect on regional median river flow trends. Consequently, the results suggest that the simulated effects of historical radiative forcing on the climate system are essential for explaining the observed patterns of regional median low, mean, and high river flows.

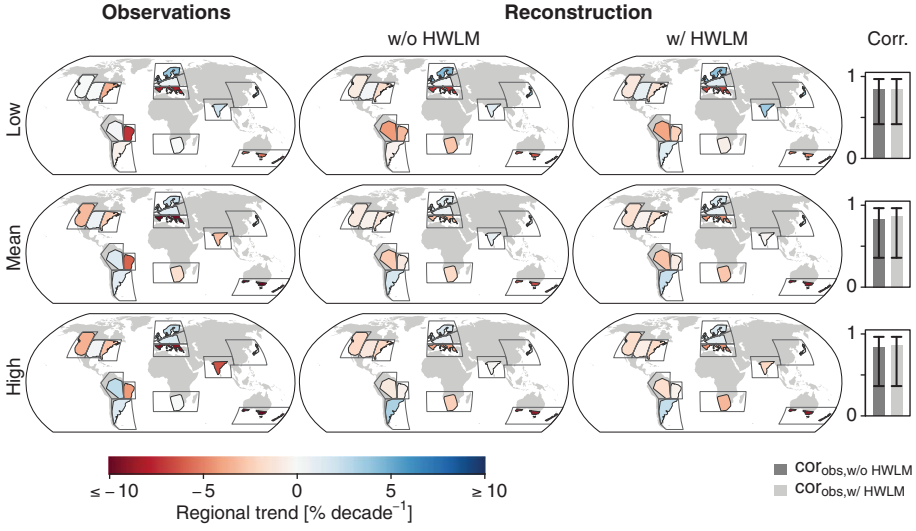

Fig. 1. Comparison of observed and reconstructed regional median river flow trends (1971–2010). "Observations" represent trends computed from in situ observations. "Reconstruction" represents multimodel mean trend of global hydrology model simulations driven by observational atmospheric forcing, with (w/) and without (w/o) the effects of HWLM. Hollow polygons indicate predefined regions used for grouping stations. Colored polygons are defined by the convex hull around the station coordinates in the respective regions. Colors indicate the regional median trend. The color scale for the trends has been truncated to enhance the readability of the maps. Figure S9 displays the full range of all data presented here. The plots labeled "Corr." show Pearson correlation coefficients between the spatial patterns of observed and reconstructed regional median trends, alongside 99% confidence intervals that are based on Fisher's z transform.

To investigate effects of the mismatch between point-scale observatories and model grid cells and to assess impacts of regional sampling biases of the observations, the analysis was repeated using GHM-based river flow reconstructions that allow for full spatial coverage (figs. S2 to S7). Despite additional uncertainties induced by model-based reconstructions, the results are widely consistent with the observational assessment (fig. S8). Furthermore, a detailed inspection of observed, reconstructed, and simulated trends shows that the internal variability implied by HIST&HWLM simulations is comparable to observed variability (figs. S9 to S12), indicating the validity of the assumption that natural climate variability can be approximated through chaotic model trajectories.

We note that as in any climate change detection and attribution exercise, we cannot fully rule out that processes not captured by the models might contribute to the observed trend pattern (*32*). For example, there remain uncertainties regarding the response of transpiration to dryness stress or in the representation of HWLM. Furthermore, although the ISIMIP2b ensemble allows HWLM to be accounted for in a climate change detection and attribution setup for the first time, the fact that no separate simulations with either anthropogenic or historical natural forcing are available hinders an unambiguous attribution of the observed trend pattern to ACC. In particular, natural changes in the radiative forcing triggered by large volcanic eruptions have been shown to affect the global hydrological cycle. However, recent research has demonstrated that the effects of such eruptions on river flow are typically confined to a few years after the eruption (*34*) and are therefore expected to only have a small influence on long-term trends.

Overall, the presented analysis lines up with the existing body of literature documenting that ACC is influencing the world's water cycle (*4*–*6*, *16*–*20*). Possible mechanisms that drive trends in low, mean, and high river flow include large-scale shifts in precipitation (*4*, *5*, *17*), changes in factors that influence evapotranspiration (*6*, *19*, *20*), and alterations of the timing of snow accumulation and melt driven by rising temperatures (*8*, *12*). Combining the evidence of these findings with the results of the presented analysis (Figs. 1 and 2) supports the conclusion that it is likely that ACC is contributing to the global pattern of trends in low, mean, and high river flow.

We demonstrate for the first time that the global pattern of observed changes in river flow are only captured by model simulations that account for historical radiative forcing

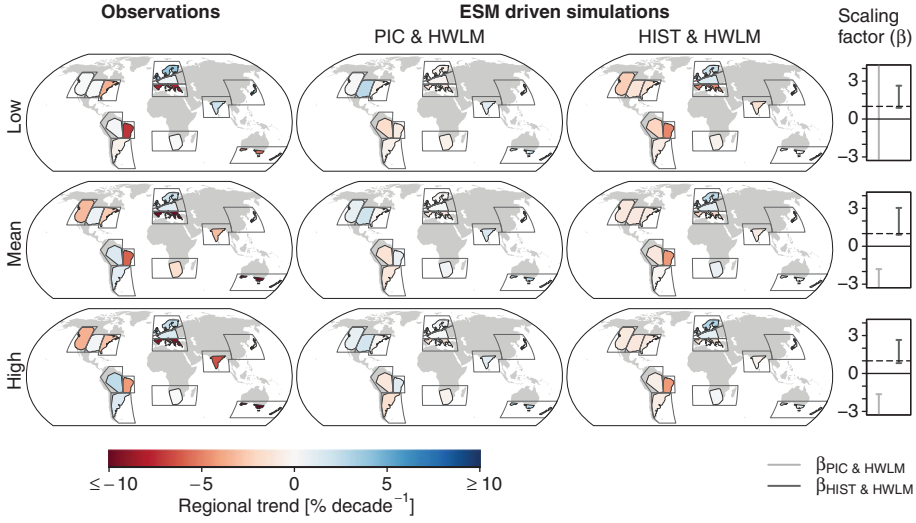

Fig. 2. Comparison of observed and simulated river flow trends (1971–2010). "Observations" are the same as in Fig. 1 and included here to facilitate comparison. "ESM-driven simulations" represent trends computed from model experiments that account for HWLM but consider simulated atmospheric data with either preindustrial (PIC) or historical (HIST) radiative forcing. The color scale for the trends has been truncated to enhance the readability of the maps. Figures S9 and S10 display the full range of all data presented here. The scaling factor plots show 10 to 90% confidence intervals of the scaling factors from the detection analysis. The simulated patterns are consistent with the observations if the lower bound of the confidence interval is larger than zero (solid horizontal line). The magnitude of observed and simulated change is consistent if the confidence intervals include one (dashed horizontal line). Confidence intervals exceeding the range of the ordinate are truncated to enhance readability of the plot.

and that simulated effects of HWLM do not substantially contribute to explaining global trend patterns of low, mean, and high flows. Thus, we have provided clear evidence for the role of historical radiative forcing as a causal driver of trends in mean and extreme river flow at the global scale.

REFERENCES AND NOTES

1. P. Greve, L. Gudmundsson, S. I. Seneviratne, *Earth Syst. Dyn.* **9**, 227–240 (2018).
2. Y. Hirabayashi *et al.*, *Nat. Clim. Chang.* **3**, 816–821 (2013).
3. C. Prudhomme *et al.*, *Proc. Natl. Acad. Sci. U.S.A.* **111**, 3262–3267 (2014).
4. X. Zhang *et al.*, *Nature* **448**, 461–465 (2007).
5. K. Marvel, C. Bonfils, *Proc. Natl. Acad. Sci. U.S.A.* **110**, 19301–19306 (2013).
6. K. M. Willett, N. P. Gillett, P. D. Jones, P. W. Thorne, *Nature* **449**, 710–712 (2007).
7. L. Gudmundsson, S. I. Seneviratne, X. Zhang, *Nat. Clim. Chang.* **7**, 813–816 (2017).
8. T. P. Barnett *et al.*, *Science* **319**, 1080–1083 (2008).
9. G. Blöschl *et al.*, *Nature* **573**, 108–111 (2019).
10. G. Blöschl *et al.*, *Science* **357**, 588–590 (2017).
11. C. Rosenzweig *et al.*, *Nature* **453**, 353–357 (2008).
12. H. G. Hidalgo *et al.*, *J. Clim.* **22**, 3838–3855 (2009).
13. F. Jaramillo, G. Destouni, *Science* **350**, 1248–1251 (2015).
14. P. C. D. Milly, K. A. Dunne, A. V. Vecchia, *Nature* **438**, 347–350 (2005).
15. P. Wu, R. Wood, P. Stott, *Geophys. Res. Lett.* **32**, L02703 (2005).
16. X. Gu *et al.*, *Geophys. Res. Lett.* **46**, 2573–2582 (2019).
17. K. Marvel *et al.*, *Nature* **569**, 59–65 (2019).
18. B. Mueller, X. Zhang, *Clim. Change* **134**, 255–267 (2016).
19. H. Douville, A. Ribes, B. Decharme, R. Alkama, J. Sheffield, *Nat. Clim. Chang.* **3**, 59–62 (2012).
20. R. S. Padrón *et al.*, *Nat. Geosci.* **13**, 477–481 (2020).
21. C. J. Vörösmarty, P. Green, J. Salisbury, R. B. Lammers, *Science* **289**, 284–288 (2000).
22. I. Haddeland *et al.*, *Proc. Natl. Acad. Sci. U.S.A.* **111**, 3251–3256 (2014).
23. H. X. Do, L. Gudmundsson, M. Leonard, S. Westra, *Earth Syst. Sci. Data* **10**, 765–785 (2018).
24. L. Gudmundsson, H. X. Do, M. Leonard, S. Westra, *Earth Syst. Sci. Data* **10**, 787–804 (2018).
25. K. Frieler *et al.*, *Geosci. Model Dev.* **10**, 4321–4345 (2017).
26. Materials and methods are available as supplementary materials.
27. S. I. Seneviratne *et al.*, in *Managing the Risks of Extreme Events and Disasters to Advance Climate Change Adaptation: Special Report of the Intergovernmental Panel on Climate Change*, C. B. Field *et al.*, Eds. (Cambridge Univ. Press, 2012), pp. 109-230.
28. M. R. Allen, P. A. Stott, *Clim. Dyn.* **21**, 477–491 (2003).
29. L. Gudmundsson, M. Leonard, H. X. Do, S. Westra, S. I. Seneviratne, *Geophys. Res. Lett.* **46**, 756–766 (2019).
30. S. Gosling *et al.*, ISIMIP2a Simulation Data from Water (global) Sector (V. 1.1). GFZ Data Services (2019); https://doi.org/10.5880/PIK.2019.003.
31. T. I. E. Veldkamp *et al.*, *Environ. Res. Lett.* **13**, 055008 (2018).
32. N. L. Bindoff *et al.*, in *Climate Change 2013: The Physical Science Basis. Working Group I Contribution to the Fifth Assessment Report of the Intergovernmental Panel on Climate Change*, T. F. Stocker *et al.*, Eds. (Cambridge Univ. Press, 2013), pp. 867–952.
33. A. Hannart, A. Ribes, P. Naveau, *Geophys. Res. Lett.* **41**, 1261–1268 (2014).
34. C. E. Iles, G. C. Hegerl, *Nat. Geosci.* **8**, 838–842 (2015).
35. L. Gudmundsson, H. X. Do, M. Leonard, S. Westra, The Global Streamflow Indices and Metadata Archive (GSIM) – Part 2: Time series indices and homogeneity assessment. PANGAEA (2018); https://doi.org/10.1594/PANGAEA.887470.

ACKNOWLEDGMENTS

Funding: We acknowledge financial support as follows: L.G. and S.I.S. were supported through the H2020 projects CRESCENDO (grant no. 641816) and 4C (grant no. 821003). S.I.S. acknowledges support from the European Research Council through the ERC DROUGHT-HEAT project (grant no. FP7-IDEAS-ERC-617518). H.M.S. is supported in part by the German Federal Ministry of Education and Research (BMBF, grant no. 01LS1711F). H.X.D. is supported by the University of Michigan (grant no. U064474). W.T. acknowledges support from the Uniscientia Foundation and the ETH Zurich Foundation (grant no. Fel-45 15-1). J.L. is supported by the National Natural Science Foundation of China (grant nos. 41625001 and 41571022) and the Strategic Priority Research Program of Chinese Academy of Sciences (grant no. XDA20060402). J.B. acknowledges support from MEXT/JSPS KAKENHI (grant no. 16H06291) and the Environmental Research and Technology Development Fund (grant no. 2RF-1802). Y.P. acknowledges support from the National Science Foundation (grant no. 1752729). Y.S. was supported by the Ministry of Education, Culture, Sports, Science and Technology of Japan (Integrated Research Program for Advancing Climate Models) (grant no. JPMXD0717935715). M.G.G. received support from the Greek State Scholarship Foundation (IKY) (grant no. MIS5033021). **Author contributions**: L.G. conceptualized the study, conducted the data analysis, and drafted the paper with contributions from all co-authors. H.M.S., J.B., W.T., and Y.S. conducted model simulations contributing to the ISIMIP ensembles. S.N.G. and H.M.S. coordinated the ISIMIP model simulations. **Competing interests:** The authors declare no competing interests. **Data and materials availability**: Observed river flow indices can be downloaded from PANGAEA (*35*). The model-based data are freely available through the ISIMIP project [ISIMIP2a: available through GFZ Data Services (*30*); ISIMIP2b: available at https://esgf-data.dkrz.de/projects/esgf-dkrz/].

SUPPLEMENTARY MATERIALS

science.sciencemag.org/content/371/6534/1159/suppl/DC1
Materials and Methods
Figs. S1 to S12
Tables S1 to S7
References (*36*–*44*)

29 November 2019; accepted 25 January 2021
10.1126/science.aba3996

Globally observed trends in mean and extreme river flow attributed to climate change

Lukas Gudmundsson, Julien Boulange, Hong X. Do, Simon N. Gosling, Manolis G. Grillakis, Aristeidis G. Koutroulis, Michael Leonard, Junguo Liu, Hannes Müller Schmied, Lamprini Papadimitriou, Yadu Pokhrel, Sonia I. Seneviratne, Yusuke Satoh, Wim Thiery, Seth Westra, Xuebin Zhang and Fang Zhao

Science **371** (6534), 1159-1162.
DOI: 10.1126/science.aba3996

Change of flow

Anthropogenic influence on climate has changed temperatures, precipitation, atmospheric circulation, and many other related physical processes, but has it changed river flow as well? Gudmundsson *et al.* analyzed thousands of time series of river flows and hydrological extremes across the globe and compared them with model simulations of the terrestrial water cycle (see the Perspective by Hall and Perdigão). They found that the observed trends can only be explained if the effects of climate change are included. Their analysis shows that human influence on climate has affected the magnitude of low, mean, and high river flows on a global scale.

Science, this issue p. 1159; see also p. 1096